Spin and parity determination of the 3.004-MeV level in ^{27}Al: Its low-lying multiplet structure

T. Shizuma,[1] M. Omer,[2,*] R. Hajima,[1] N. Shimizu,[3] and Y. Utsuno[4]

[1]*Tokai Quantum Beam Science Center, National Institutes for Quantum and Radiological Science and Technology, Tokai, Ibaraki 319-1106, Japan*

[2]*Integrated Support Center for Nuclear Nonproliferation and Nuclear Security, Japan Atomic Energy Agency, Tokai, Ibaraki 319-1195, Japan*

[3]*Center for Nuclear Study, University of Tokyo, Hongo, Bunkyo-ku, Tokyo 113-0033, Japan*

[4]*Advanced Science Research Center, Japan Atomic Energy Agency, Tokai, Ibaraki 319-1195, Japan*

(Received 20 December 2018; published 10 July 2019)

The spin and parity of the 3.004-MeV level in ^{27}Al have been determined by measuring the angular correlation function of radiation emitted from levels populated by resonant absorption of polarized photons. The nuclear resonance fluorescence experiments were carried out at the High Intensity γ-ray Source (HIγS) facility at Duke University using quasimonoenergetic linearly polarized photon beams. The spin and parity of levels in ^{27}Al were deduced from a comparison of the measured angular distribution ratios and azimuthal intensity asymmetries with theoretical predictions. The observed resonance properties were compared with shell model calculations using the universal *sd* interaction. Monte Carlo shell model calculations were also performed to investigate the low-energy structure of ^{27}Al.

DOI: 10.1103/PhysRevC.100.014307

I. INTRODUCTION

The spin assignment of the 3.004-MeV level in ^{27}Al has an influence on the interpretation of the low-energy structure of ^{27}Al. Previous experiments have given spin $J = 9/2$ to this level from inelastic neutron [1] and proton [2] scattering, and γ-ray angular correlations using a ^{26}Mg(p,γ) reaction [3]. The spin-parity $J^\pi = 11/2^+$ level at 5.500-MeV decays most intensely by a strong mixed $E2/M1$ transition with a multipole mixing ratio of 0.29(2) to the level at 3.004 MeV, which itself is known to decay by $E2$ radiation to the $J^\pi = 5/2^+$ ground state [4]. This uniquely leaves the spin-parity assignment $J^\pi = 9/2^+$ as the only possibility. Despite the firm spin assignment of $J = 9/2$, Angell *et al.* [5] recently claimed a spin assignment of $J = 7/2$ by measuring the integrated cross section of the 3.004-MeV transition in nuclear resonance fluorescence (NRF) experiments with a circularly polarized photon beam.

Several macroscopic models were used to investigate the low-energy structure of ^{27}Al. The weak coupling model [6] considered the spin-parity $J^\pi = 9/2^+$, 3.004-MeV state as one resulted from the coupling of a $d_{5/2}$ proton hole to the first excited 2^+ state of the ^{28}Si core. The strong coupling model [7,8], in contrast, predicted a $J = 7/2$ state near 3 MeV as the second member of the $K^\pi = 5/2^+$ ground state band. The $J = 9/2$ assignment for the 3.004-MeV level was the most problematic issue for this model. Furthermore, the rotational-vibrational coupling model [9] interpreted the $J^\pi = 9/2^+$, 3.004-MeV state as a head of a $K = 9/2$ γ-vibrational band (a $d_{5/2}$ proton hole coupled to the $K = 2$ γ-vibrational core) where K is the projection of angular momentum on the symmetry axis in deformed nuclei. On the other hand, microscopic calculations based on the nuclear shell model in the *sd*-shell region predicted a $J = 9/2$ level within 30 keV of the 3.004-MeV level [10,11]. Reliable and accurate information on the spin and parity of the 3.004-MeV level is required for further theoretical investigations.

It has been shown that a quasimonochromatic, linearly polarized photon beam produced by laser Compton scattering (LCS) considerably increases experimental sensitivities, particularly for the determination of both spin and parity of resonantly excited levels [12–15]. In the present work, NRF measurements using such a photon beam were performed to investigate low-lying states in ^{27}Al. The measured intensity asymmetry of the scattered γ rays with respect to the polarization of incident photons as well as the angular distribution ratio was used to determine spin and parity of levels in ^{27}Al in a model-independent fashion [16], as the NRF occurs only via electro-magnetic interactions. The transition strength was also deduced from the measured scattering intensity. The present results are compared with those obtained via shell model calculations using the universal *sd* (USD) interaction [10,11]. The intrinsic shapes of the low-energy levels of ^{27}Al are also investigated by using the "T-plot" of the Monte Carlo shell model (MCSM) [17,18].

II. EXPERIMENTAL PROCEDURE

The present NRF measurements were performed at the High Intensity γ-ray Source (HIγS) facility at the Free-Electron Laser (FEL) Laboratory, Duke University in Durham, NC, USA [19]. The ^{27}Al 2.982- and 3.004-MeV levels were simultaneously excited by NRF using the high-flux (1.8×10^7 γ/s) linearly polarized quasi-monoenergetic

*Permanent address: Physics Department, Faculty of Science, Assiut University, Assiut 71516, Egypt.

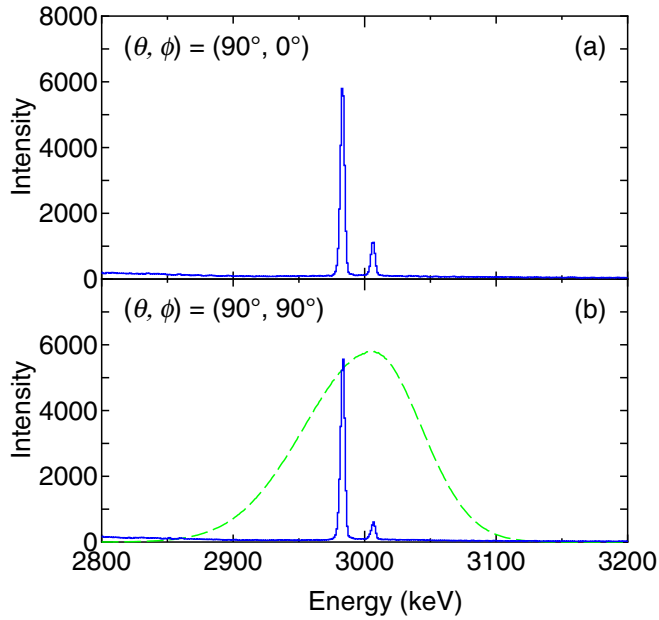

FIG. 1. Photon scattering spectra measured at polar and azimuthal angles of $(\theta, \phi) = (90^\circ, 0^\circ)$ and $(90^\circ, 90^\circ)$. The beam profile is overlaid (not to scale) as a broken line in the lower panel.

γ-ray beam. The beam irradiated an Al target with a thickness of 25 mm and a diameter of 32 mm, placed in an evacuated plastic tube to reduce the background counts due to scattering of the incident photons by air. The NRF γ rays were detected with six high-purity germanium (HPGe) detectors with 55% and 60% relative to the 3×3 in^2 NaI scintillator detector. Four of the six HPGe detectors were positioned at a scattering angle $\theta = 90^\circ$ relative to the beam with azimuthal angles $\phi = 0^\circ$, 90° 180°, and 270°, such that two of the detectors were in the horizontal plane in parallel to the polarization axis of the beam and the other two were in the vertical plane. The other two HPGe detectors were placed at $\theta = 135^\circ$ with $\phi = 0^\circ$ and 270°. Note that $\phi = 0^\circ$ (90°) is equivalent to $\phi = 180^\circ$ (270°) for the present detector geometry. The distance from the center of the target to the detectors was 16.3 cm on average. Lead and copper absorbers with a thickness of 5.5 and 3.5 mm, respectively, on average were placed in front of the HPGe detectors to reduce the intensity of low energy photons hitting the detector. The detector efficiencies were measured using a calibrated ^{56}Co source.

The photon beam was collimated by a lead collimator with a length of 20 cm and a cylindrical hole with a diameter of 2.2 cm. The energy distribution of the incident photon beam was measured with a HPGe detector placed in the beam periodically during the experiment. The beam flux was reduced during these measurements by inserting Cu attenuators into the beam further upstream. The relative efficiency of the HPGe detector was 123%. A spectrum of the photon beam corrected for detector response is presented in Fig. 1(b). This HPGe detector was also used to monitor the beam flux by measuring the Compton scattering at about 13° off of a 1-mm-thick Cu plate. The details of the method are described in Ref. [5].

The angular distribution function of a γ_2 ray deexciting a level with angular momentum J_1 to a level J_2 via a mixed transition of type (L_2, L_2') where $L_2' = L_2 + 1$, relative to an absorbed polarized γ_1 ray exciting the level J_1 from a level J_0 via a mixed transition of type (L_1, L_1'), where $L_1' = L_1 + 1$ is given by [16,20,21]

$$W(\theta, \phi) = \sum_{\nu=0}^{\text{even}} B_\nu(\vec{\gamma}_1) A_\nu(\gamma_2) P_\nu(\cos\theta) + (\pm)_{L_1} \cos(2\phi) \sum_{\nu=2}^{\text{even}} B'_\nu(\vec{\gamma}_1) A_\nu(\gamma_2) P^{(2)}_\nu(\cos\theta), \tag{1}$$

where $P_\nu(\cos\theta)$ and $P^{(2)}_\nu(\cos\theta)$ are Legendre polynomials and un-normalized associated Legendre polynomials, respectively. The first term of the right-hand side of the equation is the angular distribution function for an unpolarized γ_1 ray. The factors $(\pm)_{L_1}$ are $+1$ (-1) if L_1 is of electric (magnetic) character. The expansion coefficients A_ν, B_ν, and B'_ν are given by the phase convention of Krane, Steffen, and Wheeler in Ref. [22]. Equation (1) includes multipole mixing ratios δ_1 and δ_2 for the γ_1- and γ_2-ray transitions, respectively. For the case of elastic scattering, the levels J_0 and J_2 are identical to each other so that $L_1 = L_2$ and $\delta_1 = \delta_2$.

Using the azimuthal angular distributions at $(\theta, \phi) = (90^\circ, 0^\circ)$ and $(90^\circ, 90^\circ)$, the azimuthal intensity asymmetry is defined in Ref. [12] as

$$\Sigma = \frac{W(90^\circ, 0^\circ) - W(90^\circ, 90^\circ)}{W(90^\circ, 0^\circ) + W(90^\circ, 90^\circ)}. \tag{2}$$

The corresponding intensity asymmetry of the observed NRF γ rays is given by

$$A = \frac{N_\parallel - N_\perp}{N_\parallel + N_\perp} = q\Sigma, \tag{3}$$

where $N_\parallel$ $(N_\perp)$ represents the measured intensity of NRF γ rays detected at $\theta = 90^\circ$ in the plane in parallel (perpendicular) to the polarization axis of incident photons. The value A depends on the angular momenta of the ground and excited states, the transition multipolarities, and the mixing ratios. Here, q is the experimental sensitivity, which is less than unity because of the finite solid angle of the HPGe detectors and the spatially extended target. In the present case, q is estimated to be about 0.95 for the spin sequences $5/2 \rightarrow 3/2, 5/2, 7/2$, or $9/2 \rightarrow 5/2$ by the numerical simulation assuming that the degree of polarization of the incident photon beam is nearly 100%.

We also use the angular distribution ratio $R = W(90^\circ)/W(135^\circ)$ for the spin determination. Here, the angular distribution function $W(\theta)$ is expressed by the first term of the right-hand side of Eq. (1). The measured angular distribution ratio is given by $N(90^\circ)/N(135^\circ)$ where $N(\theta)$ is the summation of the intensities of NRF γ rays detected at $\phi = 0^\circ$ and 270° for each scattering angle θ. The value R depends on the angular momenta of the ground and excited states and the mixing ratios. Using the azimuthal intensity asymmetry and angular distribution ratio, we determined the spin and parity of the 3.004-MeV level in ^{27}Al.

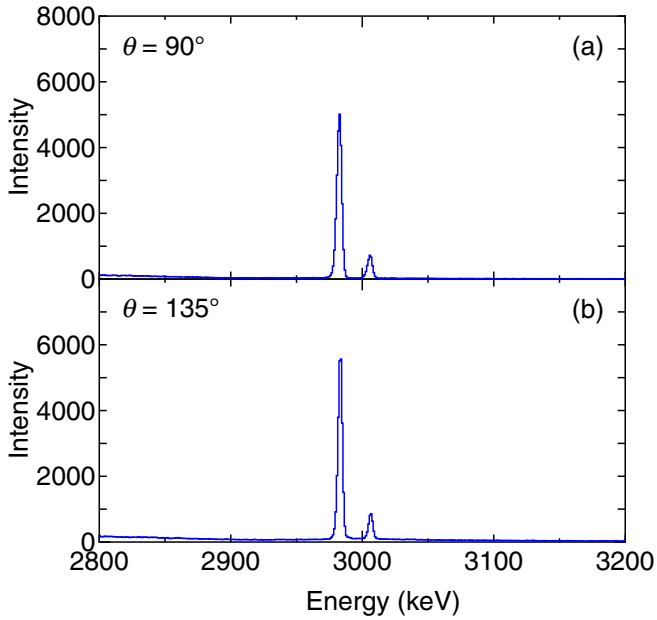

FIG. 2. Photon scattering spectra measured at $\theta = 90^\circ$ and 135°. These were obtained by summation of the spectra observed at $\phi = 0^\circ$ and 270° for each scattering angle θ.

III. RESULTS

Figures 1(a) and 1(b) present the photon scattering spectra obtained at polar and azimuthal angles $(\theta, \phi) = (90^\circ, 0^\circ)$ and $(90^\circ, 90^\circ)$, while Figs. 2(a) and 2(b) present those obtained at $\theta = 90^\circ$ and 135°. Comparison of γ-ray intensities for the 2.982- and 3.004-MeV peaks in these spectra was made to extract the azimuthal asymmetries and angular distribution ratios. The results are summarized in Table I.

The spin and parity of the 2.982-MeV level are known to be $J^\pi = 3/2^+$ [23]. Figure 3 compares the measured angular distribution ratio and the azimuthal intensity asymmetry obtained from the present measurement with those calculated for the spin sequence $5/2^+ \to 3/2^+ \to 5/2^+$ with mixing ratios δ from -1 to $+1$. The measured and calculated values are in good agreement for the vanishing mixing ratio, which is consistent with the known value $\delta = -0.01(1)$ from previous work [3]. The results for the 3.004-MeV transition are also shown in Fig. 4. From comparison with the calculations, the $J^\pi = 5/2^+$ and $7/2^+$ assignments can be excluded at

TABLE I. Results for the measured asymmetries A and angular distribution ratios R for transitions in ^{27}Al. The integrated cross sections I_s and the partial decay width to the ground state Γ_0 are also shown.

E_γ[a] (keV)	A	R	I_s (eV b)	Γ_0 (meV)
2982.0	0.02(5)	0.98(7)	31.9(7)[b]	116.7(2.5)[b]
3004.0	0.34(5)	0.95(7)	3.8(4)	$7.0^{(+8)}_{(-9)}$

[a]Transition energies E_γ taken from Ref. [23].
[b]Taken from Ref. [24].

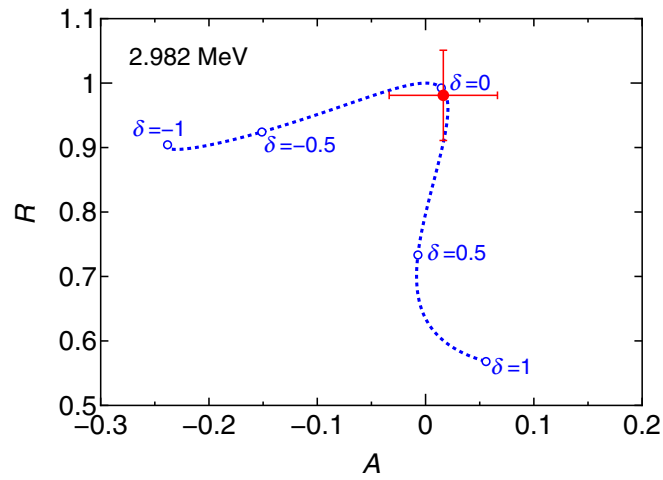

FIG. 3. Measured azimuthal asymmetry A and angular distribution ratio R for the 2.982-MeV transition is plotted with filled circles. The values calculated for the spin sequence $5/2^+ \to 3/2^+ \to 5/2^+$ with mixing ratios δ from -1 to $+1$ are plotted with a dotted line.

confidence levels of 87% (1.5σ) and 99.7% (3.0σ), respectively, but only the $J^\pi = 9/2^+$ assignment is possible for the 3.004-MeV level. Here, we assume a pure $E2$ transition, i.e., $\delta = 0$, for the $5/2^+ \to 9/2^+ \to 5/2^+$ spin sequence because a competing $M3$ transition is usually weak. The $J^\pi = 5/2^+$ assignment can be further excluded by comparison of the measured and expected integrated cross sections (see discussion below).

Since the levels were simultaneously excited (see Figs. 1 and 2), the integrated cross section I_s of the 3.004-MeV level can be determined as a ratio to the integrated cross section I_s' of the 2.982-MeV level (superscript $'$ denotes the 2.982-MeV

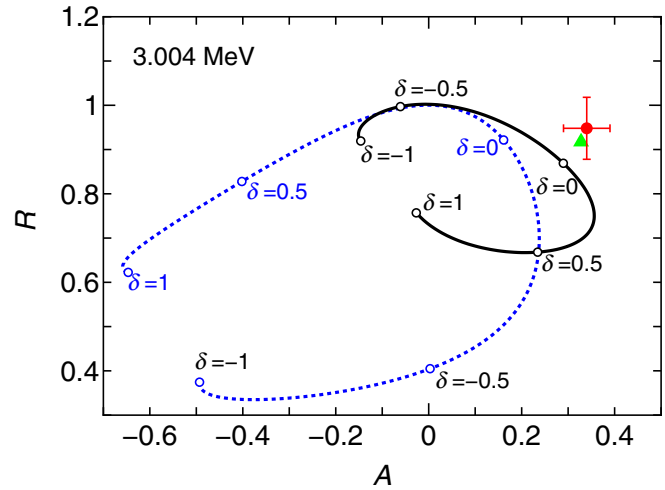

FIG. 4. Same as Fig. 3, but for the 3.004-MeV transition. The values calculated for the spin sequence $5/2^+ \to 5/2^+ \to 5/2^+$ and $5/2^+ \to 7/2^+ \to 5/2^+$ with mixing ratios δ from -1 to $+1$ are plotted with solid and dotted lines, respectively. The value calculated for the spin sequence $5/2^+ \to 9/2^+ \to 5/2^+$ with $\delta = 0$ is also plotted with filled triangle.

transition):

$$I_s = I'_s \frac{I_\gamma}{I'_\gamma} \frac{\Phi'\epsilon' W' \lambda'_{tt}}{\Phi \epsilon W \lambda_{tt}}. \quad (4)$$

Here, I_γ represents the measured intensities of the respective transitions. Φ, ϵ, and λ_{tt} are the photon flux, detection efficiency, and correction factor of atomic and self-absorption. The determination of the integrated cross section relative to that of 2.982-MeV transition has the advantage that the efficiencies of the detectors and the photon flux are needed in relative units only.

The correction factor λ_{tt} can be calculated analytically by accounting for resonance width and thermal broadening through the following equation [5,25]:

$$\lambda\left(E, N_t^w; \Gamma_0\right) = \frac{1-\exp\left\{-[\sigma_D(E;\Gamma_0)+\sigma_e(1+1/\cos\theta)]N_t^w\right\}}{[\sigma_D(E;\Gamma_0)+\sigma_e(1+1/\cos\theta)]N_t^w}, \quad (5)$$

where σ_D is the thermally broadened resonance shape, Γ_0 is the resonance ground state width, σ_e is the atomic scattering cross section [26], N_t^w is the areal density of the target, and θ is the scattering angle. Equation (5) is the thick target correction for the resonance shape and must be integrated over the energy E to obtain the scaler value λ_{tt}. The equation for σ_D can be found in Ref. [25]. For the present case, λ_{tt} was obtained as 0.678 for the 2.982-MeV transition and 0.783 for the 3.004-MeV transition. Using Eq. (4) with the integrated cross section $I'_s = 31.9(7)$ eV b [24] for the 2.982-MeV transition, we obtained $I_s = 3.8(4)$ eV b for the 3.004-MeV transition.

The integrated scattering cross section I_s is related to Γ_0 according to

$$I_s = g\left(\frac{\pi\hbar c}{E_\gamma}\right)^2 \Gamma_0 b_0, \quad (6)$$

where $g = (2J_x+1)/(2J_0+1)$ is a spin factor with J_x and J_0 being the spins of the excited and ground states, respectively. E_γ and b_0 also denote the transition energy and the branching ratio to the ground state. This integrated cross section can be used to validate the spin value for the 3.004-MeV level. Using the literature values of $\Gamma_0 = 7.74(46)$ meV [24,27] and $b_0 = 0.88^{(+2)}_{(-5)}$ [23], the expected integrated cross sections can be obtained as $I_s = 2.55^{(+16)}_{(-21)}$, $3.40^{(+22)}_{(-28)}$, and $4.25^{(+27)}_{(-35)}$ for the three spin values covering the range of previously reported spins: $J = 5/2$, $7/2$, and $9/2$. There is a larger lower limit on the uncertainty reflecting the ground state branching ratio if the upper limits for unobserved branches are included. The $J = 5/2$ assignment can be excluded at a confidence level of better than 2σ by comparison with the value of $I_s = 3.8(4)$ obtained in the present measurement. By combining it with the result of the measurements of the angular distribution ratios and the azimuthal intensity asymmetries, $J^\pi = 9/2^+$ is assigned to the 3.004-MeV level with a confidence level of better than 2σ. Using Eq. (6) with $I_s = 3.8(4)$ eV b and $b_0 = 0.88^{(+2)}_{(-5)}$, we obtained $\Gamma_0 = 7.0^{(+8)}_{(-9)}$ meV for the 3.004-MeV ground-state transition. The experimental results are summarized in Table I.

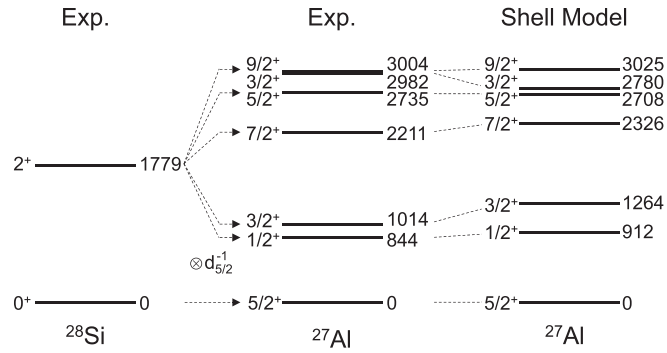

FIG. 5. Observed energy levels, shown in units of keV, of ^{27}Al in comparison with those of ^{28}Si and the shell model calculation for ^{27}Al.

The reduced transition probabilities $B(E2)\uparrow$ for excitation can be extracted from the ground state decay width Γ_0 using the following relationship:

$$B(E2)\uparrow = 1240 g \frac{\Gamma_0}{E_\gamma^5}\ [e^2\mathrm{fm}^4], \quad (7)$$

where Γ_0 is given in units of meV and E_γ in units of MeV. Applying Eq. (7) to the 3.004-MeV transition, we obtained $B(E2)\uparrow = 59(7)\ e^2\mathrm{fm}^4$. The corresponding $E2$ strength in Weisskopf units (W.u.) is 7.4(9), which indicates some collectivity. In the weak coupling model [6] low-energy states in ^{27}Al can be described by coupling a $d_{5/2}$ proton hole to the first excited 2^+ state in ^{28}Si. The present $E2$ strength can be compared with 13.2(5) W.u. [23] for the $2^+ \rightarrow 0^+$ core transition in ^{28}Si. The reduction of the strength indicates that the effects of the core state are reduced with increasing level energy and spin [28].

IV. DISCUSSION

In order to investigate low-energy structure of levels below $\approx$3 MeV in ^{27}Al, shell-model calculations were carried out in the *sd* model space with the USD [10,11] Hamiltonian. The code KSHELL [29] was used for this purpose. As shown in Fig. 5, the calculations reproduce the observed low-lying energy levels within 250 keV. We also estimated $E2$ strength for excitation to the excited levels, using the standard $E2$ effective charges $(e_p, e_n) = (1.3e, 0.5e)$ for the USD [11]. The experimentally deduced $E2$ strength of 59(7) $e^2\mathrm{fm}^4$ is in reasonable agreement with calculations that yielded $B(E2)\uparrow = 69\ e^2\mathrm{fm}^4$ within the 2σ value.

The $9/2^+$ level located at 3.004 MeV has been considered to be a member of the multiplet consisting of a proton $d_{5/2}$ hole coupled to the 2^+ state in ^{28}Si [6,9] as shown in Fig. 5. Whether or not this picture is appropriate can be examined by calculating the overlap probabilities between the calculated energy levels and the pure hole states. The overlap probabilities are represented as

$$P = \left|\left\langle \Psi\left(J_n^\pi;\ ^{27}\mathrm{Al}\right)\middle|\Phi(J^\pi)\right\rangle\right|^2, \quad (8)$$

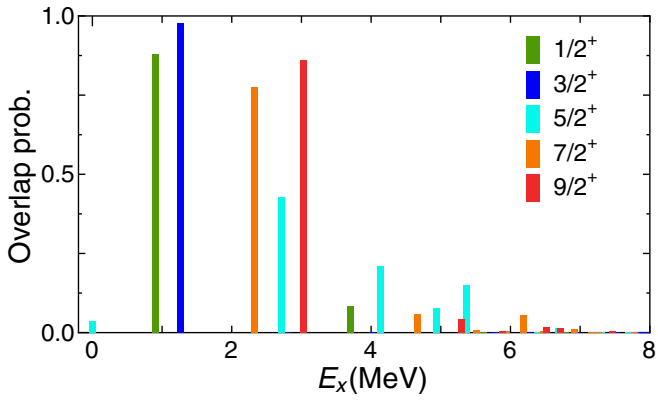

FIG. 6. Overlap probabilities of the wave functions between the states with $J^\pi = 1/2^+$ to $9/2^+$ below 8 MeV in ^{27}Al and the state obtained by coupling the first 2^+ state in ^{28}Si to a $d_{5/2}$ proton hole.

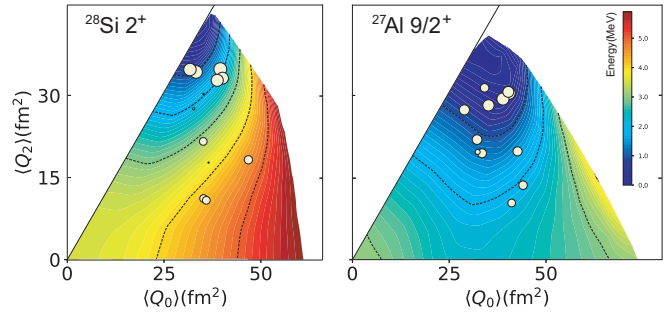

FIG. 7. T-plots of the 2^+ state of ^{28}Si and the $9/2^+$ state of ^{27}Al coordinated by intrinsic mass quadrupole moments, Q_0 and Q_2. The distribution of the MCSM basis states is depicted by circles. The locations of the circles indicate the intrinsic shape of the MCSM basis states, and the sizes denote their importance in the total wave function [18].

where $\Psi(J_n^\pi;\ ^{27}\mathrm{Al})$ is the nth eigenstate in ^{27}Al with J^π, and $\Phi(J^\pi)$ stands for the hole state expressed as

$$\Phi(J^\pi) = \mathcal{N}[a_{\pi d_{5/2}} \otimes \Psi(2^+;\ ^{28}\mathrm{Si})]^J \tag{9}$$

with the normalization constant $\mathcal{N}$ and the annihilation operator a_i. It is noted that possible J values are $1/2$ to $9/2$. Figure 6 shows the distribution of P below $E_x = 8$ MeV in ^{27}Al. While the overlap probabilities are fragmented for the $5/2^+$ states, those of the $1/2^+$, $3/2^+$, $7/2^+$, and $9/2^+$ states are concentrated in the yrast levels and are close to unity, thus supporting the multiplet picture.

The above picture can be further confirmed by comparison of the intrinsic shapes between the 2^+ state in ^{28}Si and the $1/2^+$ to $9/2^+$ states in ^{27}Al. Since the conventional shell-model calculation cannot be used to deduce the intrinsic deformation directly, we introduce the MCSM [17]. In the MCSM framework, the resultant wave function is expressed as a linear combination of the angular-momentum-projected, parity-projected Slater determinants, each of which is called an MCSM basis vector. The intrinsic deformation and its fluctuation are visualized using the intrinsic quadrupole moments of these basis vectors.

Figure 7 shows the potential energy surfaces (PESs) of the ^{28}Si and ^{27}Al as the contour lines. They are obtained by the Q-constrained Hartree-Fock method [30] using the same shell-model Hamiltonian. Both the PESs show oblate minima around $Q_0 = -60$ fm^2, which corresponds to the intrinsic electric quadrupole moment of ≈ -54 fm^2 by taking the effective charges into account. This result agrees with that extracted from the measured quadrupole moment for the 2^+ state in ^{28}Si [31], $-56(11)$ fm^2. On the PESs, the MCSM basis vectors of the 2^+ state in ^{28}Si and of the $9/2^+$ state in ^{27}Al, coordinated by intrinsic mass quadrupole moments, Q_0 and Q_2, are presented as the white circles in Fig. 7; these are called T-plots [17,18]. The basis vectors for these states are distributed around the above oblate minima with slight γ deformation. The other multiplet members with $J^\pi = 1/2^+$ to $7/2^+$ also have the similar intrinsic shapes. These results are consistent with the interpretation that the lowest excited states with $J^\pi = 1/2^+$ to $9/2^+$ in ^{27}Al are the members of the multiplet consisting of a proton $d_{5/2}$ hole coupled to the 2^+ state in ^{28}Si.

V. SUMMARY

In summary, NRF experiments on ^{27}Al were performed using a quasimonoenergetic, linearly polarized photon beam. The measured angular distribution ratios and the azimuthal asymmetries of the intensities of the γ rays scattered in the planes in parallel and perpendicular to the polarization axis of incident photons were compared with predictions. Previous experiments have given the firm spin assignment $J = 9/2$ to the 3.004-MeV level. The spin-parity $J^\pi = 11/2^+$ level at 5.500 MeV decays most intensely by a strong mixed $E2/M1$ transition with multipole mixing ratio of 0.29(2) to the level at 3.004 MeV, which itself is known to decay by $E2$ radiation to the $J^\pi = 5/2^+$ ground state. This uniquely leaves the spin-parity assignment $J^\pi = 9/2^+$ as the only possibility. The present measurement supports the spin and parity $3/2^+$ for the 2.982-MeV levelwhich is consistent with literature values. The spin and parity of the 3.004-MeV level was determined as $J^\pi = 9/2^+$, consistent with the previous work using inelastic neutron and proton scattering and ^{26}Mg(p, γ) and ^{24}Mg$(\alpha, p\gamma)$ reactions. The integrated cross section $I_s = 3.8(4)$ eV b and the reduced transition probability $B(E2)\uparrow = 59(7)\ e^2\mathrm{fm}^4$ were also obtained. The shell model calculations using the universal sd interaction reproduce the observed resonance properties of the 3.004-MeV level. From the theoretical analysis of the overlap probabilities, the 3.004-MeV level can be interpreted as the $9/2^+$ member of the multiplet resulting from the coupling of a $d_{5/2}$ proton hole to the first exited 2^+ level of ^{28}Si core. The analysis of the intrinsic shapes of the 2^+ state in ^{28}Si and the $9/2^+$ state in ^{27}Al by using the Monte Carlo shell model calculations also supports this interpretation.

ACKNOWLEDGMENTS

We would like to acknowledge the support provided by the staff at the High Intensity γ-ray Source facility. This work was a part of the study of NRF phenomenon aiming at

nuclear security and safeguards applications, being supported by the subsidiary for "promotion of strengthening nuclear security or the like" of the Ministry of Education, Culture, Sports, Science, and Technology (MEXT), Japan. The program code used in the shell-model calculations of this study was developed under efforts supported by "Priority Issue 9 to be Tackled by Using Post K Computer" from MEXT and JICFuS.

[1] J. Towle and W. Gilboy, Nucl. Phys. **39**, 300 (1962).
[2] B. Lawergren, Nucl. Phys. **53**, 417 (1964).
[3] D. M. Sheppard and C. van der Leun, Nucl. Phys. A **100**, 333 (1967).
[4] M. Lickert, J. Brenneisen, F. Glatz, D. Grathwohl, A. Martinez v. Remisowski, H. Röpke, J. Siefert, and B. H. Wildenthal, Z. Phys. A **331**, 409 (1988).
[5] C. T. Angell, R. Hajima, T. Hayakawa, T. Shizuma, H. J. Karwowski, and J. Silano, Phys. Rev. C **90**, 054315 (2014).
[6] V. K. Thankappan, Phys. Rev. **141**, 957 (1966).
[7] R. Lombard and G. Bishop, Nucl. Phys. A **101**, 601 (1967).
[8] C. L. Lin, Chin. J. Phys. **14**, 95 (1976).
[9] K. T. Knöpfle, A. Kiss, M. Rogge, U. Schwinn, P. Turek, O. Aspelund, and C. Mayer-Böricke, Phys. Rev. C **13**, 1400 (1976).
[10] B. Wildenthal, Prog. Part. Nucl. Phys. **11**, 5 (1984).
[11] B. A. Brown and B. Wildenthal, Annu. Rev. Nucl. Part. Sci. **38**, 29 (1988).
[12] N. Pietralla, Z. Berant, V. N. Litvinenko, S. Hartman, F. F. Mikhailov, I. V. Pinayev, G. Swift, M. W. Ahmed, J. H. Kelley, S. O. Nelson, R. Prior, K. Sabourov, A. P. Tonchev, and H. R. Weller, Phys. Rev. Lett. **88**, 012502 (2001).
[13] T. Shizuma, T. Hayakawa, H. Ohgaki, H. Toyokawa, T. Komatsubara, N. Kikuzawa, A. Tamii, and H. Nakada, Phys. Rev. C **78**, 061303(R) (2008).
[14] N. Pietralla, T. C. Li, M. Fritzsche, M. W. Ahmed, T. Ahn, A. Costin, J. Enders, J. Li, S. Müller, P. von Neumann-Cosel, I. V. Pinayev, V. Yu. Ponomarev, D. Savran, A. P. Tonchev, W. Tornow, H. R. Weller, V. Werner, Y. K. Wu, and A. Zilges, Phys. Lett. B **681**, 134 (2009).
[15] T. Shizuma, T. Hayakawa, H. Ohgaki, H. Toyokawa, T. Komatsubara, N. Kikuzawa, T. Inakura, M. Honma, and H. Nakada, Phys. Rev. C **87**, 024301 (2013).
[16] U. Kneissl, H. H. Pitz, and A. Zilges, Prog. Part. Nucl. Phys. **37**, 349 (1996).
[17] N. Shimizu, T. Abe, M. Honma, T. Otsuka, T. Togashi, Y. Tsunoda, Y. Utsuno, and T. Yoshida, Phys. Scr. **92**, 063001 (2017).
[18] Y. Tsunoda, T. Otsuka, N. Shimizu, M. Honma, and Y. Utsuno, Phys. Rev. C **89**, 031301(R) (2014).
[19] H. Weller *et al.*, Prog. Part. Nucl. Phys. **62**, 257 (2009).
[20] N. Pietralla, M. W. Ahmed, C. Fransen, V. N. Litvinenko, A. P. Tonchev, and H. R. Weller, in *Frontiers of Nuclear Structure*, 29 July – 2 August 2002, Berkeley, edited by P. Fallon, R. Clark, and A. M. Smith, AIP Conf. Proc. No. 656 (AIP, New York, 2003), p. 365.
[21] L. W. Fagg and S. S. Hanna, Rev. Mod. Phys. **31**, 711 (1959).
[22] K. S. Krane, R. M. Steffen, and R. M. Wheeler, Nucl. Data Tables **11**, 351 (1973).
[23] M. S. Basunia, Nucl. Data Sheets **112**, 1875 (2011).
[24] N. Pietralla, I. Bauske, O. Beck, P. von Brentano, W. Geiger, R.-D. Herzberg, U. Kneissl, J. Margraf, H. Maser, H. H. Pitz, and A. Zilges, Phys. Rev. C **51**, 1021 (1995).
[25] F. Metzger, in *Progress in Nuclear Physics*, edited by O. Frisch (Pergamon, New York, 1959), Vol. 7, p. 53–88.
[26] M. Berger *et al.*, *XCOM: Photon Cross section Database*, Technical Report (National Institute of Standards and Technology, Gaithersburg, MD, 1999).
[27] P. M. Endt, Nucl. Phys. A **521**, 1 (1990).
[28] P. Tikkanen, J. Keinonen, V. Karttunen, and A. Kuronen, Nucl. Phys. A **456**, 337 (1986).
[29] N. Shimizu, T. Mizusaki, T. Utsuno, and Y. Tsunoda, Comp. Phys. Comm. (2019), doi: 10.1016/j.cpc.2019.06.011.
[30] P. Ring and P. Schuck, *The Nuclear Many-Body Problem* (Springer, Berlin, 1980).
[31] R. H. Spear, Phys. Rep. **73**, 369 (1981).